J1.13 RESPONSE OF HIGH RESOLUTION COUPLED SEA ICE/OCEAN MODEL TO THE ASSIMILATION OF ICE MOTION FIELDS DERIVED FROM MICROWAVE SATELLITE IMAGERY

Donald Stark*
Naval Postgraduate School, Monterey, California

1 INTRODUCTION

Motivated by abundant sources of data and the need to improve weather prediction capabilities, data assimilation has a long history in atmospheric modeling. Data assimilation applied to sea-ice models, on the other hand, is in its infancy. Most of the investigations over the past twenty years falls into one of three categories: (1) the statistical interpolation of data into gridded fields (Thorndike and Colony, 1983), (2) advanced assimilation methods applied to simplified "box" style sea-ice models (Thomas and Rothrock, 1989), and (3) the non-statistical assimilation of ice data (Maslanik and Maybee, 1994). While the work of Maslanik and Maybee comes closest, no one had tackled the problem of statistically assimilating data into a full-featured sea-ice model. This situation changed with the work of Meier et al. (2000). They assimilated ice motions derived from passive microwave imagery into a fully dynamic-thermodynamic sea-ice model using optimal interpolation, a statistical interpolation technique. Their success motivated this project.

This work expands on the results of Meier by moving to a high resolution (18 km), fully coupled ice/ocean model, and improving the assimilation machinery by temporally varying the error co-variances. Two simulations with identical forcing are run for a period of five years. Both simulations use a coupled sea-ice/ocean model, but one of the simulations also includes the assimilation of ice motions. A comparison of these two simulations shows that the error in the ice motion field, subject to assimilation, is significantly reduced. This study investigates the nature of that decrease.

2 ICE MOTION DATA

In this study, two types of observational data will be used. The first is an interpolated buoy motion product generated by the Polar Remote Sensing Group at the Jet Propulsion Laboratory (JPL). The second, also from the Polar Remote Sensing Group at JPL, is a gridded ice motion product derived from passive microwave satellite images. Both ice motion products can be downloaded from the Polar Remote Sensing Group web site at ***www-radar.jpl.rgps.gov/rgps/ice_motion.html***.

2.1 BUOY DATA

A gridded ice motion product, interpolated from the International Arctic Buoy Program (IABP) buoy motions is obtained from the from Polar Remote Sensing Group. The twice daily, 100 km resolution buoy locations are converted into a gridded field of daily ice velocities. The velocity fields are then used to compute the spatial distribution of the assimilative and prognostic model error.

2.2 PASSIVE MICROWAVE DATA

The assimilation process takes an ***observed*** source of motion data and combines it with a prognostic model solution. For this study, the ice motion data or product to be assimilated is the derived passive microwave motions from JPL. These motions are derived from 85 GHz passive microwave brightness temperature fields by applying a maximum cross-correlation feature-tracking algorithm to a sequence of images (Kwok, 1998). The derived daily ice motion product has a spatial resolution of 83 1/3 km, and is available from October through the end of May. The product is not available during the summer months due to moisture contamination from cloud cover and surface melt reducing the ability of the feature tracking algorithm to differentiate ice structure in the brightness temperature field.

3 NUMERICAL MODELS

Two numerical models are used for the comparison. The first is a coupled 18 km dynamic-thermodynamic sea-ice/ocean model (Zhang et al. 1999 & Zhang and Semtner 2001). The ocean component is based on the Parallel Ocean Climate Model (POCM) of Semtner and Chervin (1992). The ocean model was adapted to the Arctic Ocean (Parsons, 1995; Maslowski, 1997) with an added free surface (Killworth et al., 1991). The second model is a combined sea-ice/ocean and assimilative model, which uses the Zhang and Semtner model as its prognostic component.

The assimilative model optimally blends the observed ice motions with the prognostic model motions through a variant of the optimal interpolation technique employed by Meier et al. (2000). Optimal interpolation (OI) is a statistical assimilation method that uses the observation and prognostic model error statistics to blend the observation and prognostic motions in a way that minimizes the error in a statistical sense.

The thermodynamic component of the sea-ice model consists of a zero-layer approximation for heat conduction through ice (Semtner, 1976) along with a surface heat budget following Parkinson and

*Corresponding author address: Donald Stark, Naval Postgraduate School, Code OC/SD, Monterey, CA 93943; email: stark@oc.nps.navy.mil

Washington (1979). The dynamic component consists of the elastic-viscous-plastic (EVP) model of Hunke and Dukowicz (1997), but employs the advection scheme of Hibler (1979).

The ice model domain is an 18 km resolution, 300 x 360 point polar stereographic mesh that covers the Arctic and GIN (Greenland, Iceland, and the Norwegian) seas. The ocean model is run at 1/6 degree horizontal resolution, with 30 vertical layers. The atmospheric forcing for the simulations is provided by the European Center for Medium-range Weather Forecasts (ECMWF) atmospheric reanalysis product for the period 1992-1993, continuing with the operational ECMWF analysis product through 1997. These 4-hourly products are first daily averaged, and then are linearly interpolated for each time step.

The models are run on the Cray C90 and the Cray SV1 at the Arctic Region Supercomputing Center (ARSC). On the SV1, the prognostic model takes 20 minutes of CPU time to integrate a single model day. The assimilative component adds about 19% to the prognostic model timing.

4 ASSIMILATION STUDY

A test period from January 1992 through June 1996 is investigated. For this period, the absolute error of the ice motions from the prognostic model and the assimilative model are compared. The error for these two products is constructed by projecting the 18 km resolution ice motion fields onto the 100 km buoy grid and then computing the ***(buoy–assimilative)*** and ***(buoy–prognostic)*** difference fields. The daily absolute error is then just the length or Euclidean norm of the respective difference vectors. In section 4.1 the daily difference vectors are averaged over a month and displayed. This shows the spatial distribution of the error on daily time-scales for a particular month. The difference field for the observed product is shown for reference. In section 4.2, a time series of the absolute error of the three products is presented to illustrate the spatial influence on the daily motion error.

4.1 SPATIAL DISTRIBUTION OF ERROR

The assimilation of the observed ice motions reduces the absolute daily error for the entire Arctic basin by over 50%. The spatial distribution of this error, as well as the error in the observed and prognostic motion products, is not uniform. The error for all three ice motion products (Figure 1) is greatest in the marginal ice zones (MIZ) of the Barents and the Greenland seas. The relative magnitude of this error, as might be expected, is least in the observed product (up to 3 cm/s) and greatest in the prognostic product (2–8 cm/s). In addition, the prognostic model error in the Chukchi Sea and off the North Slope of Alaska (Figure 1c) is large (3–7 cm/s). In fact, the magnitude of the daily prognostic error is often as large as the ice motions themselves!

The assimilative product is effectively a blend of the observed and the prognostic products and as such reflects the spatial details of the error from both. The assimilative error (Figure 1b) is largest (up to 7 cm/s) in the Greenland Sea, south of the Fram Strait. This coincides with a similar range of error in the prognostic product, and to a lesser extent (up to 3 cm/s), in the observed product. The area south of the Fram Strait is quite dynamic and the observed data is either non-existent or too inaccurate for the assimilation to overcome the prognostic model error. Further north, in the Barents Sea and north of the Fram Strait, the assimilation has the opposite impact. There the assimilation reduces the range of the prognostic error by roughly a third, from 2–6 cm/s to 1.5–4 cm/s, in spite of the larger than average observed error. In addition, the prognostic error in the Chukchi Sea is reduced by about 62%, from up to 8 cm/s in the prognostic product down to less than 3 cm/s after the assimilation. The error along the Alaska Slope is reduced by assimilation from up to 5 cm/s to less than 1.5 cm/s. A reduction of around 70%. The error in the Central Arctic is reduced by assimilation from 1.5–3 cm/s to below 1.5 cm/s. Again roughly a fifty percent reduction. In almost all cases, the error for the assimilated product is less than the prognostic error unless both the observed and the prognostic errors are large. This is precisely why the assimilated solution has localized spots of large error in the Barents Sea.

4.2 TEMPORAL BEHAVIOR OF ERROR

In the previous section, various marginal ice zones were considered. Here the temporal variability of the absolute error for the observed, the assimilated, and the prognostic products are examined for the same locations, specifically north and south of the Fram Strait, and the Barents and the Chukchi seas. Figure 2 shows a typical time series of these locations for the period from October 1992 through May 1993. Each time series is an average of the five nearest grid points. The error from the observed motions is represented with a dotted dark line, the assimilation error with a thin solid dark line, and the prognostic error with a thick gray line.

Figure 2a shows the temporal behavior of the error in a region south of the Fram Strait. From this graph it can be seen that for the brief periods where there is data available at this location, the observed error tends to be relatively small (>2.5 cm/s). Notice also that the observed error increases after April, when the spring thaw begins. The assimilative motion error for this period tends to be no worse than the prognostic error. In fact, when the observed data is actually available to assimilate, the assimilative error is often less.

Figure 2b shows the temporal behavior of the error for a region just north of the Fram Strait. For this location the distribution of days with no observed data are few and thinly spread. In addition, the observed error is moderate. Together these two factors result in the assimilative error being consistently less than the prognostic error, on average about a third less. There are two days during this period, the last week in December and the end of May, where the assimilative error reaches the maximum of 10 cm/s. Both of these

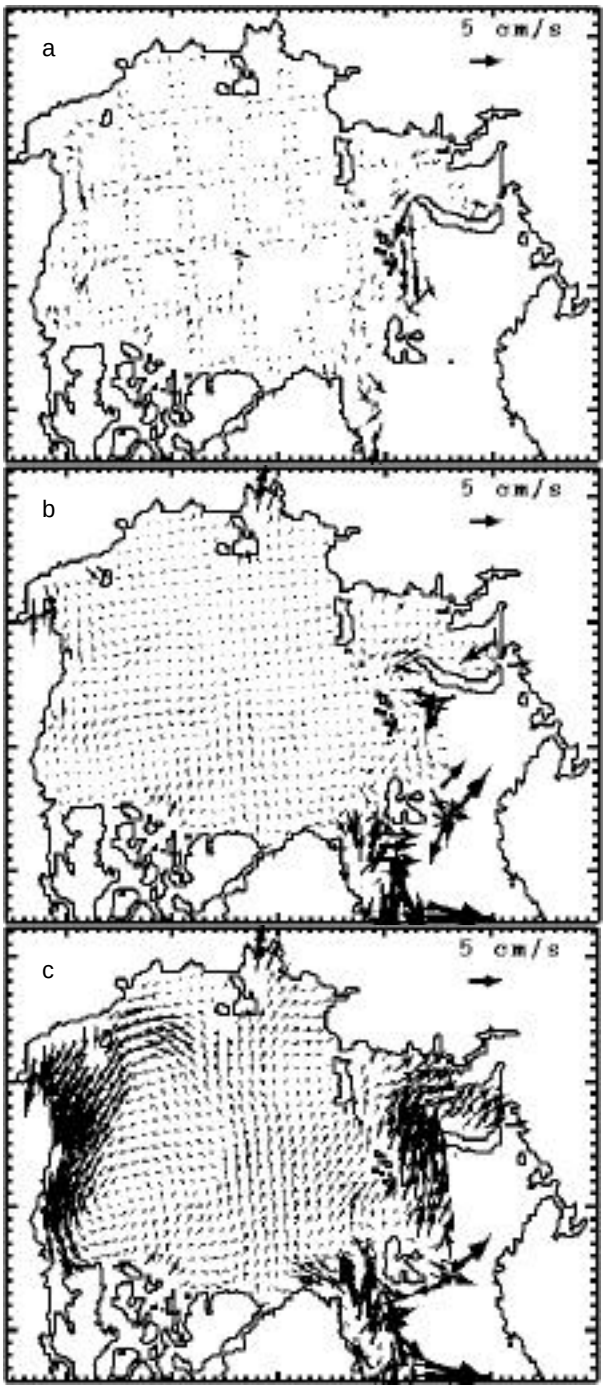

Figure 1. Typical winter example (January 1992) of a monthly average of the daily difference field with respect to buoy motions (in cm/s) for the observed product (top), the assimilated product (center), and the prognostic product (bottom). Larger arrows correspond to greater error.

events correspond to a sudden lack of observed data to assimilate, and a large prognostic error.

Figure 2c shows the temporal behavior for a region of the MIZ in the North Barents Sea. For this location, the observed data error, especially in the fall, exhibits a number of large events. In spite of this, the assimilative error is consistently better than, or at worst, the same as the prognostic error. In these cases, the observed data surrounding the location has a mitigating influence on the error.

Figure 2d shows the temporal behavior for a region in the Chukchi Sea. For this location, the assimilation exerts a strong control on the error. The average assimilative error for the eight-month period is less than half the prognostic error. The few large error events correspond to either periods of missing data or extremely large error events in the prognostic product.

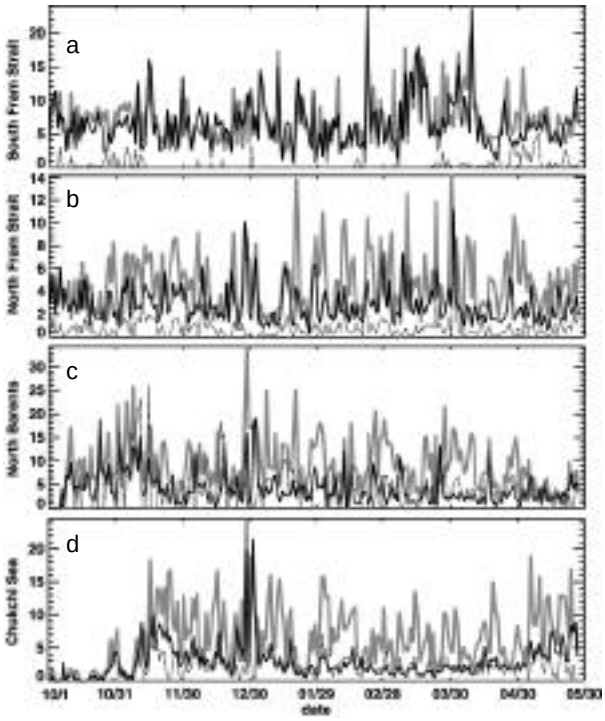

Figure 2. A typical time series of the daily absolute error (in cm/s) for October 1992 – May 1993. The assimilative (solid black), the prognostic (solid gray), and observed (dotted) errors for fixed locations in the Arctic.

5 CONCLUSION

Based on this five year study, the optimal interpolation assimilation process significantly reduces the absolute error in the ice motion field. Over the whole Arctic domain, there is a 50% reduction in the error. For the MIZ, the reduction ranges from 10–60%, with the low end being for the region south of the Fram Strait. Over monthly and longer averages, the assimilation is ***uniformly*** better than the prognostic model alone. On daily time scales, the assimilation error is ***usually*** less, and almost never worse, than the prognostic error. In the few instances where the assimilative error was worse than the prognostic error, it was by at most 1%.

The amount of error reduction is strongly a function of the error statistics of the particular geographic neighborhood. While the quality of the observed data is important, poor data or missing data is not automatically fatal. For instance, while parts of the MIZ in the GIN sea only show a marginal improvement, the MIZ in other areas, such as the Barents and Kara seas, show considerable improvement to the daily motion field.

6 REFERENCES

Hibler, W. D., 1979: A dynamic thermodynamic sea ice model, J. Phys. Oceanogr., **9**, 817-846.

Hunke, E. C., and J. K. Dukowicz, 1997: An elastic-viscous-plastic model for sea ice dynamics, J. Phys. Oceanogr., **27**, 1849-1867.

Killworth, P. D., D. Stainforth, D. J. Webb, and S. M. Peterson, 1991: The development of a free-surface Bryan-Cox-Semtner ocean model, J. Phys. Oceanogr., **21**, 1333-1348.

Kwok, R., A. Schweiger, D. A. Rothrock, S. Pang, and C. Kottmeier, 1998: Sea ice motion from satellite passive microwave imagery assessed with ERS SAR and buoy motions, J. Geophys. Res., **103(C4)**, 8191-8214.

Maslanik, J. A., and H. Maybee, 1994: Assimilating remotely-sensed data into a dynamic thermo-dynamic sea ice model, Proc. Int. Geosci. Remote Sens. Symp., Pasadena, Calif., 1306-1308.

Meier, W. N., J. A. Maslanik, and C. W. Fowler, 2000: Error analysis and assimilation of remotely sensed ice motion within an arctic sea ice model, J. Geophys. Res., **105(C2)**, 3339-3356.

Parkinson, C. L., and W. M. Washington, 1979: A large scale numerical model of sea ice, J. Geophys. Res., **84**, 311-337.

Parsons, A. R., 1995: On the Barents sea polar front in summer and interpretations of the associated regional oceanography using an Arctic ocean general circulation model, Ph.D. thesis, Naval Postgraduate School, Monterey, Calif.

Thomas, D. R., and D. A. Rothrock, 1989: Blending sequential scanning multichannel microwave radiometer and buoy data into a sea ice model, J. Geophys. Res., **94**, 10907-10920.

Thorndike, A. S., and R. Colony, 1983: Objective analysis of atmospheric pressure and sea ice motion over the Arctic Ocean, Proceedings of the 7th International Conference on Port and Ocean engineering under Arctic conditions (POAC), Vol 2, 1070-1079.

Semtner, A. J., 1976: A model for the thermodynamic growth of sea ice in numerical investigations of climate, J. Phys. Oceanogr., **6**, 379-389.

Zhang, Y., W. Maslowski, and A. J. Semtner, 1999: Impact of mesoscale ocean currents on sea ice in high-resolution arctic ice and ocean simulations, J. Geophys. Res., **104(C8)**, 18409-18429.

Zhang, Y., and A. J. Semtner, 2001: The Antarctic Circumpolar wave in a global, high-resolution, coupled ice-ocean model, Ann. of Glaciol. in press.